**Atmospheric
Measurement
Techniques**
Open Access

Discussions

COMPASS

B. Bonn et al.

Title Page

Abstract	Introduction
Conclusions	References
Tables	Figures

◀◀ ▶▶

◀ ▶

Back Close

Full Screen / Esc

Printer-friendly Version

Interactive Discussion

COMPASS – COMparative Particle formation in the Atmosphere using Simulation chamber Study techniques

B. Bonn[1], S. Sun[1,*], W. Haunold[1], R. Sitals[1], E. van Beesel[1], L. dos Santos[1], B. Nillius[1], and S. Jacobi[2]

[1]Institute for Atmospheric and Environmental Sciences, J.W. Goethe University, Altenhöferallee 1, 60438 Frankfurt/Main, Germany
[2]Hessian Agency for the Environment and Geology (HLUG), Rheingaustrasse 186, 65203 Wiesbaden, Germany
[*]now at: Department of Biogeochemistry, Max-Planck-Institute for Chemistry, Hahn-Meitner-Weg 1, 55028 Mainz, Germany

Correspondence to: B. Bonn (bonn@iau.uni-frankfurt.de)

Title Page

Abstract   Introduction

Conclusions   References

Tables   Figures

◄◄   ►►

◄   ►

Back   Close

Full Screen / Esc

Abstract

The anthropogenic influence on climate and environment has increased strongly since industrialization about 150 yr ago. The consequences for the atmosphere became more and more apparent and nowadays affect our life quality on Earth progressively. Because of that it is very important to understand the atmospheric processes, on which these effects are based on, in detail. In this study we report the set-up of a novel twin chamber technique that uses the comparative method and establishes an appropriate connection of atmospheric and laboratory methods to broaden the tools for investigations. It is designed to study the impact of certain parameters and gases on ambient processes such as particle formation online and can be applied in a large variety of conditions. The characterisation of both chambers proved that both chambers operate identically with a residence time (x_T (COMPASS 1) = 26.5 ± 0.3 min and x_T (COMPASS 2) = 26.6 ± 0.4 min) at a typical flow rate of 15 L min^{-1} and a deposition rate $(1.6 \pm 0.8) \times 10^{-5}$ s^{-1}. Comparison measurement showed no significant differences. Therefore operation under atmospheric conditions is trustworthy. To indicate the applicability and the benefit of the system a set of experiments was conducted at different conditions, i.e. urban and remote, enhancing ozone and terpenes as well as reducing sunlight. In the ozone enhanced ambient particle number and volume increased substantially at urban and remote conditions in a different strength. Solar radiation displayed a clear positive effect on particle number as well as terpene addition did at remote conditions. Therefore the system is a useful tool to investigate local precursors, the details of ambient particle formation at surface locations as well as future feedback processes.

1 Introduction

The change of climate conditions on regional and global scale has been reported and is established (IPCC, 2007, 2013). In this context certain aspects such as temperature, radiation budgets, volatile organic compounds and ozone will change differently on different scales. In order to understand and approximate certain effects and their feedback on climate in an appropriate way novel tools are needed to link laboratory detailed techniques and ambient long term observations.

Both approaches include strong benefits and some weaknesses: among the benefits of laboratory studies the following aspects can be named exemplarily: controlled conditions, investigations under suitable conditions, application of measurement techniques under homogeneous conditions and facilitation of a detailed process based simulation because of the fixation of well-known boundary conditions. The disadvantages include primarily the elevated concentration used for precursor gases and the limitation in process evolution time. Ambient measurements allow the determination of a wide range of different conditions and their annual pattern. However, due to the spot-like measurements that are affected by transport and local sources and sinks and the time resolution of instruments separation of individual aspects are challenging in the highly nested atmospheric system. This gap is aimed to be addressed by our new comparative twin chamber COMPASS that facilitates the usage of laboratory tools in a certain time frame under ambient conditions. Based on this approach the increase of future temperature or of gases can be investigated as well as the impact of certain anthropogenically enhanced species. In this study the construction, characterization and exemplary application for a well-known ambient problem is explained.

This well-known problem concerns the ambient new aerosol particle formation processes from gaseous precursors, which have been observed all around the globe (Kulmala et al., 2004c) and which have been studied since more than a century. A wide range of theories have been developed for explanation, which include primarily sulfuric acid related mechanisms such as binary and ternary nucleation (Kulmala et al., 2004b).

These are expected to take place in the free troposphere and in the vicinity of significant ammonia sources such as agriculture and farming (Korhonen et al., 1999; Spracklen et al., 2010). Others like the ion-induced nucleation (Hirsikko et al., 2011; Kirkby et al., 2012) or the iodine oxide related oligomerization (Burkholder et al., 2004) have been demonstrated to be relevant for the upper troposphere or the coastal zones, whereas algae emissions of diiodomethane (CH_2I_2) occur at draught stress conditions (O'Dowd and Hoffmann, 2005). In the case of coastal new particle formation the emitted volatile organic compounds (VOCs) subsequently react with ambient ozone and start the process of new aerosol particle production. Besides the mentioned ones several further theories have been postulated (Ryding et al., 2012; Bonn and Moortgat, 2003; Bonn et al., 2008) but could not be proven by aerosol mass spectrometry techniques (Jimenez et al., 2009) as the corresponding particular mass is too small and particles undergo chemical transformation during accumulation. This problem is severe, since only very tiny amounts (perhaps less than a pptv) of a compound are required to create a new phase, if the compound of interest has the right physic-chemical properties, i.e. low-volatility, notable interaction with other species or a high chemical reactivity. Nevertheless, once the new particles are formed a significant fraction grows beyond the size at which they can act as cloud condensation nuclei (CCN) and alter the physical size distribution of cloud droplets. This has a remarkable impact on the radiation budget in the climate system (Kulmala et al., 2004a; Merikanto et al., 2009) and provides the key uncertainty in predicting climate feedbacks and processes. Therefore a novel technique for investigating these processes is needed.

So far most of the so-called nucleation studies have been performed under controlled laboratory conditions with sometimes enhanced precursor concentrations to speed up the formation and early growth. The concluding results are then used to interpret ambient observations and processes, an aspect that is object to criticism. In this study we report a novel technique that uses the comparative method and provides a mixture between atmospheric and laboratory methods. It is designed to study the impact of certain parameters and gases online and can be applied in a large variety of conditions.

2 Material and methods

2.1 Construction

The construction of two identical twin chambers aims to measure atmospheric situations at two identical conditions except one parameter to investigate its impact of on the
5 process observed. It shall allow a notable residence time to investigate slowly occurring processes and it aims to reduce dry deposition to its minimum and the surface to be chemically inert. Thus both twin chambers shall alter ambient conditions to a minimum stage.

Therefore the surface material is made of ethylene tetrafluoroethylene (ETFE, Texlon
10 GmbH). It has a high level of transparency in the UV region (100 % of UV-A and 50 % of UV-C), is inert and very resistant against chemical reactive substances like ozone and is temperature resistant up to 150 degrees Celsius. The material is weather proof (wind, temperature and rain) and the selected foil has a thickness of 25 µm.

The scaffold of the twin chambers is made of stainless steel with a total height of
15 3 m, which stabilizes the chamber towers on the right and left sides of the scaffold with several carrier rings (Fig. 1). The foothold material is formed as two rings each, i.e. one on the outside and one inside. Each outer (carrier) ring is fixed on the scaffold and its diameter can be narrowed by a screw to fix the foil between outer and inner ring. The foil is welded vertically to a cylinder. This cylindrical main section of each chamber
20 has a total height of 1.8 m and a diameter of 50 cm. At the inlet and outlet region of the chamber the cylindrical form is reduced concentrically. Above and below the main section the diameter of the cylinder reduces from 50 to 15 cm in both, i.e. upper and lower, parts. The reduction of the inlet diameter aims to focus the direction of the inlet stream and to minimize the influence of turbulence. Mounted at the top is an inlet tube
25 consisting of acrylic glass, which is connected to a cover plate with a flange. Finally a flexible aluminium tube bended towards the ground is fixed at each of the chambers to protect them from rain.

In the following one of the chambers is used as a reference (COMPASS 1) while the second one (COMPASS 2) is modified as desired. Therefore COMPASS 2 has an additional glass inlet for adding gases.

The chamber outlet is situated in the center of the flow tube at the lowest part of the chamber. Two different outlet lines for gases and aerosol particles are chosen to prevent destruction of chemicals in the conducting tubes for the aerosol particle analysis. The flow dynamics are kept laminar with a Reynolds number Re of 420 and can be expected as simulated using the FLUENT 6.1 software (Fig. 2) for $15\,\mathrm{L\,min^{-1}}$. The total flow rate in each chamber is controlled by mass flow controllers and electrical pumps. To allow sampling with a minimum of instrumentation both chamber outlets (COMPASS 1 and 2) for gases and particles are connected to electrical switches (gases: magnetic valve, Bückert, particles: OSE-KKP, Grotec) controlled by a Labview card (National Instruments) and program that switches in 5 min intervals between both chambers ($\Delta t = 10$ min). To guarantee that the flow is stable while the changing time of the magnetic valve there is a second magnetic valve, which is coupled with the first one. On this way an additional pump with the same flow rate like the gas measurement device can stabilize the flow of that chamber, which is current uncoupled from the gas measurement.

2.2 Instrumentation for measurements

2.2.1 Gaseous and meteorological measurements

Temperature and relative humidity are measured by Hygrosens sensors (Model: HYTE-ANA-10V, Hygrosens) at the end of each chamber in 5 s intervals. The comparison of both sensors at controlled laboratory conditions yielded no significant difference outside the measurement uncertainty. Both chambers are constructed identical to compare the data afterward on a relative scale. Ozone was detected using the Horiba APOA-350E instrument alternatively in COMPASS 1 and 2. Its sampling flow was set to $1\,\mathrm{L\,min^{-1}}$ and the measurement range was chosen to fit best to the range of expected

values. For volatile organic compounds a high-sensitivity proton transfer reaction mass spectrometer (HS-PTR-MS, Ionicon, Innsbruck, Austria) was applied and was operated in the same line as the ozone sample. Important masses were selected by running a mass scan at the start of each set-up. Chosen masses were either significantly different in both chamber samples or were selected because of significant local sources. The sampling time for the individual masses was adapted to the present mixing ratio range, i.e. the smaller the longer resulting in a total time resolution between 32 and 37.4 s. For more details the reader is referred to Bourtsoukidis et al. (2012).

2.2.2 Particle phase measurements

In order to physically characterize the ambient particle number and mass concentration two different set-ups were applied: (a) for quantification of the total aerosol number concentration a buthanol based coundensation particle counter (CPC, TSI 3025A, TSI Inc., USA) with a lower cut-off size of 2.7 nm in diameter was used and averaged for 30 s intervals. Flows were calibrated before application and regularly afterwards. (b) To measure the particle volume and mass as well the system was extended to a scanning mobility particle sizer (SMPS, TSI 3936, TSI Inc., USA). This instrument was configured as follows: sample flow = $1.5 \, \text{L min}^{-1}$ (high flow), sheath flow = $6.0 \, \text{L min}^{-1}$, particle density assumed to be $1.2 \, \text{g cm}^{-3}$ and two scans per sample with 120 s upscan and 15 s downscan. These times result in a total sampling time of the SMPS per sample of 4 min 30 s. The remaining 30 s for a total of 5 min interval the SMPS was set to pause in order to prevent measurements during the switch from one to the other chamber.

To maintain the total flow rates in both chambers identical a set of 4 flow controllers was used. Since gas and particle phase measurements took place in alternating chambers with a match of the total flow rates of gases and of aerosol particles ($1.5 \, \text{L min}^{-1}$) the corresponding residual flows were selected accordingly.

2.2.3 Data analysis and intercomparison

Since the focus is set to the relatively compare both chamber results, each parameter measurements were divided into datasets for the individual chambers using the recorded valve switching times and the MATLAB software (Mathworks Inc.). Subsequently all values between 30 s and 4:30 min after switching were averaged. The mean values were used to calculate the ratio of value (COMPASS 2)/value(COMPASS 1) using the COMPASS 2 interval following the COMPASS 1 interval, which is the first by starting the magnetic and the GROTEC valves. This assumes that no significant change occurs in any chamber in smaller time steps than 5 min.

3 Results

3.1 Determination of chamber residence time

Due to the unreactive properties of CO_2 it was used as a trace gas to determinate the residence time inside the chamber. The gas was added into the inlet region of the chamber from a specific time on. At the outlet region the time-dependent rising of the CO_2 mixing ratio was measured by a CO_2-measruement device (BIOS[®] 100). The 50 % change-time between the initial and the final CO_2-mixing value was taken as the residence time for gases and aerosol particles in the center area of the chambers covered by the hopper-shaped outlet. An exponential fit of the normalized CO_2-data vs. time was added to calculate the residence time with following function:

$$y = A_1 \exp\left(-\frac{x}{t_1}\right) + y_0 \tag{1}$$

$$x_\tau = -\ln\left(\frac{y - y_0}{A_1}\right) \cdot t_1 \tag{2}$$

x represents the measured time, y the normalized CO_2 mixing ratio, y_0 the normalized initial CO_2 mixing ratio A_1 and t_1 are fitting parameters. The residence time x_τ can be calculated by Eq. (2) assuming $y = 0.5$ and $y_0 = 0$ by application of the fitting values from Eq. (1) (Fig. 3).

The derived residence time $x\tau$ was found to change between 22 and 36 min as flows varied between 10 and 20 L min^{-1} (Table 1). In this context the value at 10 L min^{-1} (COMPASS 1) was excluded from further analysis because of the heat exhaust of an oven closed by that was turned on during this particular measurement. Using all residence time values except the discarded one the relation between flow rate and mean residence time for both identical chambers the relation between residence time and flow rate follows to:

$$x_\tau = \frac{(264.0 \pm 11.7)L}{\text{flow rate}} + (9.3 \pm 0.8)\text{min} \tag{3}$$

The used residence time for ambient measurements at 15 L min^{-1} was derived as (26.5 ± 0.3) min for the reference chamber COMPASS 1 and (26.6 ± 0.4) min for the measurement chamber COMPASS 2. This facilitates about 30 min of process modification inside to study impacts.

3.2 Determination of the deposition rate at the foil surface

3.2.1 Gas dry deposition rate

The reduction of a chemically inert trace gas between inlet and outlet is based on gaseous diffusion an dry deposition to the chamber walls if the trace gas is not notably sticky and gets lost on aerosol surfaces. In this case an identical sampling line has been used to measure the relative reduction of the CO_2 mixing ratio from the inlet to outlet. The deposition rate is described by the following equation (Seinfeld and Pandis, 2006):

$$\text{vmr}_{CO_2} = \text{vmr}_{0,CO_2} \cdot \exp(-k_{\text{dep,gas}} \cdot x_\tau) \tag{4}$$

with: $vmr_{CO_2} = CO_2$ – volume mixing ratio at inlet; $vmr_{0,CO_2} = CO_2$ volume mixing ratio at outlet; $k_{dep,gas}$ = dry gas-phase deposition rate; and x_τ = residence time.

Restructuring Eq. (4) the variable k_{dep} results in:

$$k_{dep,gas} = \ln \left(\frac{vmr_{0,CO_2}}{vmr_{CO_2}} \right) \cdot \frac{1}{x_\tau} \tag{5}$$

With this the mean $k_{dep,gas}$ was obtained as $(1.3 \pm 0.6) \times 10^{-5}\,s^{-1}$. Both chambers show identical results within the range of uncertainty having values that are in the range of laboratory derived values.

3.2.2 Particle deposition rate

For determining the particle dry deposition rate the same approach as in case of the gas deposition rate was applied for individual particle sizes:

$$C_{particle}(D_p) = C_{0,particle}(D_p) \cdot \exp(-k_{dep,part} \cdot x_\tau) \tag{6}$$

with: $C_{particle}$ = particle concentration at outlet; $C_{0,particle}$ = particle concentration at inlet (aerosol dynamic corrected); $k_{dep,part}$ = deposition rate (particle s^{-1}); and x_τ = residence time (s).

And again $k_{dep,part}$ follows to

$$k_{dep,part}(D_p) = \ln \left(\frac{C_{0,particle}(D_p)}{C_{particle}(D_p)} \right) \cdot \frac{1}{x_\tau} \tag{7}$$

Due to the residence time of 26.6 min at a flow rate of $15\,L\,min^{-1}$ inside any chamber notable aerosol dynamics will affect particle concentrations. Those include the formation, coagulation and coalescence as well as the loss of particles and will have effects on the size distributions to be corrected for intercomparison purposes. However, since

the local formation of particles still remains an aspect not fully understood and might be partially related to traffic emissions this process is assumed to compensate the surface losses in the smallest size range most. Because of that the size range below 50 nm in diameter was excluded from the fitting. Because of the relevance of aerosol dynamic contributions, the dynamical effect was calculated using an aerosol dynamics box model (Jacobson, 2005) in MATLAB 2009 (MathWorks Inc., USA). The model was initialized with the aerosol size distribution gained at the inlet from ambient air at Campus Riedberg and calculated in 1 s time steps for the entire residence time in the corresponding chamber. The size distribution derived from the aerosol dynamics computations after the residence time period therefore replaces the initial particle concentration in Eq. (7) to quantify the particle deposition onto the foil surface.

Figure 4 displays a maximum of particle loss at a size range of 40 nm in particle diameter. The loss value is $(56 \pm 5)\%$ at COMPASS 1 and $(48 \pm 5)\%$ at COMPASS 2 using ambient aerosol particles and individual measurements each. The differences may partially originate from a non-stable initial aerosol and therefore different diffusion mixing within the two chambers. However, the values of both chambers display no significant difference (Fig. 5). Therefore, the fit of the mean values between 50 and 422 nm in particle diameter is provided. Since ambient air was used for testing smaller particles may be affected by new particle formation and subsequent growth in both chambers (see above). Therefore, the size range of potential effects is excluded from the fit.

Above, the deposition rate declines to a minimum at nearly 250 nm. The average fit curve for both chambers is provided:

$$k_{\text{dep,part}} = 3.46 \times 10^{-4}\ \text{s}^{-1} \cdot (\log_{10}(D_p(\text{nm})) - 2.226)^2 + 3.255 \times 10^{-4}\ \text{s}^{-1} \qquad (8)$$

This means that particles in such a size range passage the chamber with the smallest loss.

3.3 Intercomparison measurement period

The intercomparison of both chambers at ambient conditions took place without any modifications in one of the chambers during September 2013 at Campus Riedberg of Frankfurt University. The results are displayed in Fig. 6. No difference is visible in both size distribution measurements (top and center plot) as well as in total particle number concentration (bottom graph) and in particle volume for more than two days at a variety of ambient conditions. Therefore both chambers are considered to work identically.

The top and center plots in Fig. 6 show the dN/dlog(D_p)-observations in COMPASS 1 and 2 during the comparison-experiment between both chambers at a particle size range from 9.65 to 422 nm. The particle formation processes at morning and evening are obvious in the time range 269 to 270. It has the typical shape of a nucleation curve, which is also known as "banana plot". On the other hand the particle concentration about noontime is quite less. This experiment was accomplished near by the anthropogenic contaminated traffic road next to the institute. So it is rather likely that the particle formation process is mainly influenced by exhaust gas of automobile. In this case the primary chemical substances are BTEX, NO_x, SO_2 and PAKs.

The bottom graph in Fig. 6 shows the time dependent particle concentration of both chambers. The maximal particle concentration is about evening time at 3×10^4 particles cm^{-3}. In contrast the minimal particle concentration is about noontime at 5000–10^4 particles cm^{-3}. The condition of higher traffic intensity at the rush hour is supposed to control the height of the particle concentration at this time. In addition the uncertainty regions of both data series are overlapped continuously. So there are no significant differences between the measured particle concentrations of both chambers.

4   Comparative measurements

For testing and investigation purposes the novel twin chamber set-up was applied at two different environments: (a) in the urban environment of Frankfurt/Main at the university campus Riedberg (September/October 2012) and (b) in the remote biogenically affected area at Taunus Observatory (Mt. Kleiner Feldberg, 825 m a.s.l.) at a spruce forest site during spring 2013.

4.1   Urban environment (Frankfurt/Main)

The experiment conducted in Frankfurt was operated in two phases: Phase I addressed an artificial rise in ambient ozone by positioning a pen-ray lamp with a wave length of 253.7 nm in COMPASS 2 with a protection for the lamps light for the reference chamber. Phase II focussed on the impact of solar radiation by covering COMPASS 2 with aluminium foil to prevent radiation to enter and heat to penetrate inside.

4.1.1   Ozone experiment

The impact of ozone was investigated between DOY 287.5 to 288.5 and during a repetition in late November. The ozone mixing ratio climbed to values of 700–800 ppbv in the modification chamber 2 and particle number concentrations increased up to a tenfold concentration compared to the reference chamber 1 (Fig. 7). It is of interest that the particular enrichment does not only occur at day- but also at night-time, although the ozone value enrichment was generally smaller than the maximum during 287 at noon (800 ppbv). A repetition in November showed similar but weaker increases in ozone as well as in number concentrations indicating different source strength of precursors and smaller reaction rates. The volume concentration displayed a similar pattern and behaviour as the number concentration. However the increase at ozone enrichment was less intense.

Figure 7 shows the measured ozone mixing ratio (panel a), particle concentration (panel b) and particle volume concentration (panel c) while the ozone-experiment. In Fig. 7a an increase of the ozone mixing ratio is observed in COMPASS 2 to a maximum of nearly 700 ppbv. In contrast of that the ozone mixing ratio in COMPASS 1, which is measuring continuously under atmospheric background condition, stays at a quite less level around 30 ppbv. The maximal ozone mixing ratio in COMPASS 2 is about the time period DOY 287.5. After that it decreases to nearly 100 ppbv, which is still higher than the ozone mixing ratio in COMPASS 1 by factor of 3. In case of the particle concentration (Fig. 7b) there are no differences at the time period DOY 286–287.5, where the ozone mixing ratio was not increased. With the addition of ozone to COMPASS 2 an increasing of the particle concentration up to a maximum of 10^5 particles per cm^3 was observed. For COMPASS 1 the particle concentration stayed at quite small levels. The significance of the increase is apparent between both data series.

In case of the particle volume concentration there is an identical trend of rising like the particle concentration. The volume concentration in the COMPASS 2 is significantly higher than in COMPASS 2 during the ozone enrichment period.

Figure 9 shows the cross-correlation between the difference of particle concentration and ozone mixing ratio in both chamber. A clearly correlation between these two parameters is observed with the maximal cross-correlation coefficient of 0.9 at a time shift of (0.34 ± 0.17) h or (20 ± 10) min. The values of time shift above 0.34 h correspond to times, at which the residence time of 26 min inside the chamber was exceeded. The scatter plot of ozone concentration ratio of both chambers vs. particle number concentration ratio indicates a linear rise by a factor of 2.8 ± 0.3 for Frankfurt city at the start of October 2012. This means that if ozone increases by 10 % the particle number concentration would rise by about 30 % stating that ozone is an important pollutant and precursor for ambient particles.

4.1.2 Impact of solar radiation

A further impact factor for – especially urban – particle formation is solar radiation, since it controls atmospheric transport and chemical reactions. While OH is formed with increasing radiation several products degrade in its presence. In order to investigate this effect the modification chamber 2 was covered by an aluminium foil to prevent (a) the penetration of sunlight and (b) a temperature increase of the covered chamber due to isolation. In fact the chamber was found to be significantly cooler during the day (50 °C, not shaded measurement!) than the reference chamber (20 °C in darkened chamber) and with identical temperatures at night. Consequently the saturation vapour pressure of aerosol phase affine compounds drops and the chemical lifetime of reactive aerosol species increases. On the contrary new potential aerosol material is formed by hydroxyl radical reactions in the reference chamber. Comparing the importance of both aspects, the OH contribution seems evidently more important for (a) the number but also for (b) mass and volume although warmer temperatures were present (Fig. 10). Both are reduced in the covered chamber (COMPASS 2) compared to the reference one (COMPASS 1) except during night when no difference between both chambers could be found. This is in line with the expectations.

Both investigations in the urban area of Frankfurt clearly demonstrate that ozone and solar radiation lead to an enhanced particle number and mass concentration, i.e. issues for public health and therefore potential future problems.

4.2 Remote region: Taunus Observatory, spruce forest

4.2.1 Impact of solar radiation and ozone

For investigating the local effect of ozone on new particle formation a pen-ray with a wavelength maximum at 253.7 nm was mounted at the inlet of COMPASS 2 and shielded in the direction of the reference chamber COMPASS 1 in an identical way as for urban experiments.

Title Page

Abstract | Introduction

Conclusions | References

Tables | Figures

Back | Close

Full Screen / Esc

Printer-friendly Version

Interactive Discussion

In this period of observation two phases were chosen: Phase I – only ozone was enriched and Phase II – ozone was enriched and radiation reduced in COMPASS 2.

Phase I – Ozone enrichment

Because of the pen-ray lamp the ozone value in COMPASS 2 was kept constant above 100 ppbv: at minimum 1.5 to threefold of the ambient mixing ratio in COMPASS 1). There was only a moderate increase at night time i.e. especially during periods with a relative humidity close to 100 % and the most intense during day time at driest environmental conditions. The ambient ozone mixing ratio itself displayed a typical daily cycle varying between 30 ppbv at minimum and 60 ppbv at maximum (mean: 47.9 ± 6.1 ppbv) in the reference chamber. The temperature in both chambers was $18.1 \pm 6.2\,°C$ and no significant difference was observed between both enclosures ($\Delta T = 0.4 \pm 0.6\,°C$). The same applies for the relative humidity RH that was measured as $59 \pm 26\,\%$ with a difference of $\Delta\,RH = 0 \pm 2\,\%$.

Particles

With respect to total particle number concentration N above 3 nm in diameter the observations are evident. In any case ozone is significantly enhanced (Fig. 11a) the total particle number concentration increased remarkably (ca. +75 %/ppbv of ozone increase, Fig. 11b). While temperatures and relative humidity in both chambers are measured identical (Fig. 11c) and no indication for a difference in solar radiation is available, the presence of ozone and thus a subsequent reaction with an aerosol particle precursor gas evidently causes the increase. In some occasion the measured particle number concentration even exceeded the upper detection limit of the particle counter ($10^5\,\#\,cm^{-3}$) (Fig. 11b) and no further rise could be quantified.

COMPASS

B. Bonn et al.

Gases

When enhancing only ozone several oxidative VOCs presumably oxidation products of terpenoids such as mono- and sesquiterpenes indicate a clear rise (Table 3): form- and acetaldehyde, acetone and the molar mass 72 (potentially propene, butanal or butanone). Formic acid increases while acetic acid decreases. No clear change is observable for mono- and sesquiterpenes although a tendency for reduction is apparent. This can be understood especially for sesquiterpenes because of its primary constituent β-caryophyllene and the short atmospheric lifetime of less than a minute and the scattering of observations around detection limit (ca. 10–20 pptv). These reactive gases will not pass the enclosure. But the notable increase of oxidation products within the residence time of ca. 27 min within the chambers indicates a notable chemical conversion and time for further growth. The surrounding forest is no predominant isoprene emitter, i.e. spruce and so a difference of very small mixing ratios is hardly detectable.

Phase II – Ozone enrichment and solar radiation reduction

Particles

Increasing ozone and reducing solar radiation the situation appears similar as in the case of ozone only (Fig. 12). There is still a rise in total number. Although the length of the dataset is less extensive than for the ozone only experiment (Phase I) the same characteristics are apparent. Both factors, i.e. ozone and solar radiation seem important for the observed increase. In order to quantify the individual contributions the correlation coefficient ρ has been calculated for the rise in ozone as well as the present radiation in COMPASS 1 (reference) and the particle number increase. Both values show a significant dependency: $\rho(\Delta O_3, \Delta N) = 73.8 \pm 0.4$ at no time difference and ρ (radiation, ΔN) = 79.6 ± 0.3 at identical time. However the correlation increases up to a time shift (radiation earlier) by about 2.7 h to a value of 83.9 ± 0.3. This indicates

an earlier production of precursor gases by radiation or radiation initiated chemistry (OH) waiting for some ideal conditions such as nuclei that can be activated. Thus, the ozone effect, where the correlation clearly declines with time shift between rise in ozone and in particles, is the limiting step. This becomes obvious in Fig. 13, where the relative particle number enhancement in the case of the ozone only experiment is splitted into different times of the day (day- and night-time). The day-time data display a higher slope (ca. +100 % per ppbv of ozone) than the night-time one (ca. +17 % per ppbv ozone), again indicating the importance of solar radiation potentially for OH and further radical production but perhaps not during the residence time in the flowchambers. In this context it is interesting to note that the increase by ozone seems to occur primarily above ca. 35 ppbv of ambient ozone. This indicates a link to the ozone stress related emission of sesquiterpenes (Bourtsoukidis et al., 2012).

Gases

In this phase i.e. reduction of solar radiation the observations were slightly different to the previous one (Table 3). Although both smallest aldehydes are observed to increase in the presence of ozone too, methanol is clearly reduced. Terpenes and their larger oxidation products only provide a tendency for reduction of terpenes and increase of oxidation products that is in line with enhanced ozone mixing ratios and presumably intensified atmospheric reactions in chamber 2. It is worth mentioning that the presence of NO_x may cause notable contributions of the nitrate radical reactions in the dark (solar radiation reduction, chamber 2).

4.2.2 Impact of BVOCs

To test the influence of volatile organic compounds (VOCs) and their oxidation products on particle formation, two different biogenic VOCs have been selected: (1) the monoterpene ($C_{10}H_{16}$) β-pinene, which is expected to react primarily with ambient OH-radicals (approximated daily average: ca. 80 % oxidation by OH), and (2) the sesquiterpene

$(C_{15}H_{24})$ β-caryophyllene that is known to be quickly oxidized by the present ozone molecules (ca. 95 % of total sink). Next to the addition, the monoterpene is expected to start reacting with either of the two radicals (day-time: OH, night-time: NO_3). This leads to the formation of large organic peroxy radicals (RO_2) and several longer lived products such as nopinone. On the contrary the sesquiterpene will react with ambient ozone forming a large variety of products such as e.g. the Criegee intermediates (Criegee, 1975) and the intramolecularly formed secondary ozonide (Beck et al., 2011). Both BVOCs were added in a small bypass air flow of $(10 \pm 1)\,cm^3\,min^{-1}$ to COMPASS 2 using a permeation oven at a defined temperature. The oven temperature was set to $(29 \pm 0.2)\,°C$ in the case of the monoterpene (Phase III) and to $(47.8 \pm 0.2)\,°C$ in the case of the sesquiterpene (Phase IV). Both compounds were monitored by the PTR-MS instrument at the outlet of the chamber.

During both terpene additions related phases III and IV temperatures and humidity in both chambers were identical within the measurement uncertainties. This is why we will focus primarily on the gaseous i.e. VOC measurements. The VOCs measured by PTR-MS displayed several significant changes. Those are shortly summarized in Table 4 and will be discussed in the corresponding "Gases" sections the following.

Phase III – monoterpene addition

Gases

While a clear rise in monoterpene signal could be observed in Phase III (Table 4, left), further VOCs indicated a clear rise either during night-time or the entire time as well. The ones increasing all the time were methanol and mass 66 g mole (pres. cyclo-pentadiene or malononitrile), while formaldehyde, isoprene and toluene only displayed a significant change during night-time. All of these observations may result from three different processes: (i) increased production by a specific monoterpene compared to a mixture of monoterpenes in the atmosphere, (ii) a change in local sink intensity i.e. no significant reaction with ambient NO_3 but with OH and finally (iii)

lower source intensities i.e. lower emission and meteorological transport at night-time. Further masses indicated trends but remained below the range of significance (one standard deviation) such as nopinone.

Phase IV – sesquiterpene addition

5 *Gases*

In the case of sesquiterpene addition no significant changes have been monitored for any VOC (Table 4, right). However, the ozone mixing ratio dropped due to the reaction with the sesquiterpene. Because of the very short lifetime of β-caryophyllene
10 (ca. 45 s.) the increase was assumed to be identical with the drop in the ozone mixing ratio. Our observations indicate a rise between 0 and (4.5 ± 1.5) ppbv. As for monoterpene addition several masses, i.e. presumable oxidation products of β-caryophyllene with ozone displayed trends (e.g. in formaldehyde) but remained within the uncertainty range. Since the competitors in the case of ozone reacts are minor the effects were
15 found to be not significant for other VOCs. But oxidation products with ozone are expected to be rather non-volatile and effects will primarily occur in the aerosol phase.

Particles

20 It's very interesting to see the different impact of both terpenes on the ambient particle number concentration (Figs. 14–16). While the monoterpene addition displays a clear daily profile with a maximum increase around noon $(+20 \pm 5\%)$ at the most intense radiation and evidently no change at night-time conditions (Figs. 14 and 16), the sesquiterpene implies a nearly constant increase by about $+13 \pm 4\%$ except the
25 time between 10 p.m. and 2 a.m. (Figs. 15 and 16). The observations may be explained by a two stage process that can be limited at both stages, i.e. the cluster production or the activation. From our observations during the addition of the monoterpene one is tended to say that their OH oxidation production take place in the activation stage.

On the contrary the sesquiterpene-ozone production may contribute earlier and lack in activation around midnight, where favourable compounds such as OH- or NO_3-driven products display a minimum. Because of that secondary oxidation products which are important for aerosol mass production will be formed less (Li et al., 2011).

This shows evidence that both BVOCs take place in the ambient particle formation process. However the stage of impact, i.e. in the cluster formation steps or the activation of clusters, cannot be elucidated by the current measurements, since the available aerosol instrumentation was insufficient for that. This requires detailed future studies with either ion instruments or a CPC battery in the smallest size range of particles. Nevertheless, the difference in daily pattern is in agreement with the assumption of a stable cluster pool production below 2.7 nm in diameter and a solar radiation (OH) driven activation of these clusters.

5 Conclusions

The novel twin-chamber technique COMPASS has been shown to act as an appropriate tool to investigate the impact and the role of different parameters and gases in the particle formation process under a variety of different conditions. The system is not necessarily limited to particles but can be operated for cloud nuclei or gas-phase studies as well. The magnitude of the observed change depends on the residence time required for the particular process studied. This can be achieved by flow variation between 2 min (Re = 1150) and tenths of minutes, limited by the required sample flow rates. The flow system provides a laminar flow field as shown by FLUENT simulations and uses two identical chambers for the evaluation of results, i.e. one reference and one experimental chamber to modify. Because of the parallel operating chambers deposition is a minor process and its contribution will become important only at long residence times. Characterisations of both individual chambers demonstrated no significant change between both. Therefore it is evident, that both function in an identical

manner and that their application for measurements under atmospheric conditions is reasonable.

First tests in urban and forest conditions have been conducted, which indicate a strong potential for applications, i.e. starting with figuring out the important gases for the earliest cluster formation, the activation and subsequent growth, and the set-up can be applied for studying the effects on ambient particles directly in the ambient not in the laboratory at reasonable concentrations.

Experiments in the urban air of Frankfurt clearly demonstrated the formation potential of particular number and mass based on ozone and solar radiation. Therefore one can estimate a potential rise in particle mass during ozone episodes and a prospective future rise in a warmer climate.

Based on our measurements in urban and forested regions an important role of ozone in new particle formation is evident. Suppressing solar radiation reduced the measured particle number and volume concentration. However, when overlapping both changes, i.e. ozone enhancement and radiation reduction, ozone seems dominant and may produce precursor gases or activating gases via an alternative pathway such as via NO_3 production. Adding volatile organic compounds (VOCs) such as mono- and sesquiterpenes lead to a clear rise in particle number depending on the primary oxidant and the time of the day. While the monoterpene β-pinene reacts primarily with OH the particle enhancement displays the same pattern as solar radiation. On the contrary the sesquiterpene β-caryophyllene is oxidised by ozone resulting in a constant production of new particles. Important to note is the minimum at midnight although ozone remains fairly constant. However the nitrogen oxides decline and the nitrate radical production is drastically reduced. This may explain that although clusters are available the ozone oxidation products are incapable to activate those on their own without a radical initiated activation. Since these new particles will grow further to sizes at which they alter the Earths radiation budget via cloud microphysics the understanding of the processes involved are key aspects to elucidate future climate changes.

This demonstrates the wide range of the measurements possible required understanding more of the environmental processes affecting health, climate and feedback processes. The novel chamber seems to be an appropriate tool for that.

References

Atkinson, R., Baulch, D. L., Cox, R. A., Crowley, J. N., Hampson, R. F., Hynes, R. G., Jenkin, M. E., Rossi, M. J., Troe, J., and IUPAC Subcommittee: Evaluated kinetic and photochemical data for atmospheric chemistry: Volume II – gas phase reactions of organic species, Atmos. Chem. Phys., 6, 3625–4055, doi:10.5194/acp-6-3625-2006, 2006.

Beck, M., Winterhalter, R., Herrmann, F., and Moortgat, G. K.: The gas-phase ozonolysis of α-humulene, Phys. Chem. Chem. Phys., 13, 10970–11001, 2011.

Bonn, B., Schuster, G., und Moortgat, G.: Influence of water vapor on the process of new particle formation during monoterpene ozonolysis, J. Phys. Chem., 106, 2869–2881, 2002.

Bonn, B., Korhonen, H., Petäjä, T., Boy, M., and Kulmala, M.: Understanding the formation of biogenic secondary organic aerosol from α-pinene in smog chamber studies: role of organic peroxy radicals, Atmos. Chem. Phys. Discuss., 7, 3901–3939, doi:10.5194/acpd-7-3901-2007, 2007.

Bonn, B., Kulmala, M. , Riipinen, I., Sihto, S.-L., and Ruuskanen, T. M.: How biogenic terpenes govern the correlation between sulfuric acid concentrations and new particle formation, J. Geophys. Res., 113, D12209, doi:10.1029/2007JD009327, 2008.

Bonn, B., Boy, M., Kulmala, M., Groth, A., Trawny, K., Borchert, S., and Jacobi, S.: A new parametrization for ambient particle formation over coniferous forests and its potential implications for the future, Atmos. Chem. Phys., 9, 8079–8090, doi:10.5194/acp-9-8079-2009, 2009.

Burkholder, J. B., Curtius, J., Ravishankara, A. R., and Lovejoy, E. R.: Laboratory studies of the homogeneous nucleation of iodine oxides, Atmos. Chem. Phys., 4, 19–34, doi:10.5194/acp-4-19-2004, 2004.

Criegee, R.: Mechanismus der Ozonolyse, Angew. Chem., 87, 765–771, doi:10.1002/ange.19750872104, 1975 (in German).

Field, C. B., Barros, V., Stocker, T. F., Qin, D., Dokken, D. J., Ebi, K. L., Mastrandrea, M. D., Mach, K. J., Plattner, G.-K., Allen, S. K., Tignor, M., and Midgley, P. M. (Eds.): IPCC special report: Managing the Risks of Extreme Events and Disasters to Advance Climate Change Adaptation, Cambridge Univ. Press, Cambridge, UK, 2012.

Hirsikko, A., Nieminen, T., Gagné, S., Lehtipalo, K., Manninen, H. E., Ehn, M., Hõrrak, U., Kerminen, V.-M., Laakso, L., McMurry, P. H., Mirme, A., Mirme, S., Petäjä, T., Tammet, H., Vakkari, V., Vana, M., and Kulmala, M.: Atmospheric ions and nucleation: a review of observations, Atmos. Chem. Phys., 11, 767–798, doi:10.5194/acp-11-767-2011, 2011.

Jimenez, J. L., Canagaratna, M. R., Donahue, N. M., Prevot, A. S. H., Zhang, Q., Kroll, J. H., DeCarlo, P. F., Allan, J. D., Coe, H., Ng, N. L., Aiken, A. C., Docherty, K. S., Ulbrich, I. M., Grieshop, A. P., Robinson, A. L., Duplissy, J., Smith, J. D., Wilson, K. R., Lanz, V. A., Hueglin, C., Sun, Y. L., Tian, J., Laaksonen, A., Raatikainen, T., Rautiainen, J., Vaattovaara, P., Ehn, M., Kulmala, M., Tomlinson, J. M., Collins, D. R., Cubison, M. J., Dunlea, E. J., Huffman, J. A., Onasch, T. B., Alfarra, M. R., Williams, P. I., Bower, K., Kondo, Y., Schneider, J., Drewnick, F., Borrmann, S., Weimer, S., Demerjian, K., Salcedo, D., Cottrell, L., Griffin, R., Takami, A., Miyoshi, T., Hatakeyama, S., Shimono, A., Sun, J. Y., Zhang, Y. M., Dzepina, K., Kimmel, J. R., Sueper, D., Jayne, J. T., Herndon, S. C., Trimborn, A. M., Williams, L. R., Wood, E. C., Middlebrook, A. M., Kolb, C. E., Baltensperger, U., and Worsnop, D. R.: Evolution of Organic Aerosols in the Atmosphere, Science, 326, 1525–1529, 2009.

Kirkby, J., Curtius, J., Almeida, J., Dunne, E., Duplissy, J., Ehrhart, S., Franchin, A., Gagne, S., Ickes, L., Kürten, A., Kupc, A., Metzger, A., Riccobono, F., Rondo, L., Schobesberger, S., Tsagkogeorgas, G., Wimmer, D., Amorim, A., Bianchi, F., Breitenlechner, M., David, A., Dommen, J., Downard, A., Ehn, M., Flagan, R. C., Haider, S., Hansel, A., Hauser, A., Jud, W., Junninen, H., Kreissl, F., Kvashin, A., Laaksonen, A., Lehtipalo, K., Lima, J., Lovejoy, E. R., Makhmutov, V., Mathot, S., Mikkilä, J., Minginette, P., Mogo, S., Nieminen, T., Onnela, A., Pereira, P., Petäjä, T., Schnitzhofer, R., Seinfeld, J. H., Sipilä, M., Stozhkov, Y., Stratmann, F., Tome, A., Vanhanen, J., Viisanen, Y., Vrtala, A., Wagner, P. E., Walther, H., Weingartner, E., Wex, H., Winkler, P. M., Carslaw, K. S., Worsnop, D. R., Baltensperger, U., and Kulmala, M.: Role of sulphuric acid, ammonia and galactic cosmic rays in atmospheric aerosol nucleation, Nature, 476, 429–434, 2011.

COMPASS

B. Bonn et al.

Title Page

Abstract	Introduction
Conclusions	References
Tables	Figures

|◄ | ►|
◄ | ►

Back | Close

Full Screen / Esc

Printer-friendly Version

Interactive Discussion

Korhonen, P., Kulmala, M., Laaksonen, A., Viisanen, Y., McGraw, R., and Seinfeld, J.: Ternary nucleation of H_2SO_4, NH_3 and H_2O in the atmosphere, J. Geophys. Res., 104, 26349–26353, 1999.

Kulmala, M., Suni, T., Lehtinen, K. E. J., Dal Maso, M., Boy, M., Reissell, A., Rannik, Ü., Aalto, P., Keronen, P., Hakola, H., Bäck, J., Hoffmann, T., Vesala, T., and Hari, P.: A new feedback mechanism linking forests, aerosols, and climate, Atmos. Chem. Phys., 4, 557–562, doi:10.5194/acp-4-557-2004, 2004a.

Kulmala, M., Laakso, L., Lehtinen, K. E. J., Riipinen, I., Dal Maso, M., Anttila, T., Kerminen, V.-M., Hõrrak, U., Vana, M., and Tammet, H.: Initial steps of aerosol growth, Atmos. Chem. Phys., 4, 2553–2560, doi:10.5194/acp-4-2553-2004, 2004b.

Kulmala, M., Vehkamäki, H., Petäjä, T., Dal Maso, M., Lauri, A., Kerminen, V.-M., Birmili, W., and McMurry, P. H.: Formation and growth rates of ultrafine atmospheric particles: a review of observations, J. Aerosol Sci., 35, 143–176, 2004c.

Li, Y. J., Chen, Q., Guzman, M. I., Chan, C. K., and Martin, S. T.: Second-generation products contribute substantially to the particle-phase organic material produced by ?-caryophyllene ozonolysis, Atmos. Chem. Phys., 11, 121–132, doi:10.5194/acp-11-121-2011, 2011.

Merikanto, J., Spracklen, D. V., Mann, G. W., Pickering, S. J., and Carslaw, K. S.: Impact of nucleation on global CCN, Atmos. Chem. Phys., 9, 8601–8616, doi:10.5194/acp-9-8601-2009, 2009.

O'Dowd, C. D. and Hoffmann, T.: Coastal new particle formation: A review of the current stage of the art, Environ. Chem., 2, 245–255, 2005.

Pachauri, R. K. and Reisinger, A. (Eds.): IPCC 4th assessment report: Contribution of Working Groups I, II and III to the Fourth Assessment Report of the Intergovernmental Panel on Climate Change, Cambridge Univ. Press, Cambridge, UK, 2007.

Ryding, M. J., Jonsson, Å. M., Zatula, A. S., Andersson, P. U., and Uggerud, E.: Reactions of $H^+(pyridine)_m(H_2O)_n$ and $H^+(NH_3)_1(pyridine)_m(H_2O)_n$ with NH_3: experiments and kinetic modelling, Atmos. Chem. Phys., 12, 2809–2822, doi:10.5194/acp-12-2809-2012, 2012.

Spracklen, D. V., Carslaw, K. S., Merikanto, J., Mann, G. W., Reddington, C. L., Pickering, S., Ogren, J. A., Andrews, E., Baltensperger, U., Weingartner, E., Boy, M., Kulmala, M., Laakso, L., Lihavainen, H., Kivekäs, N., Komppula, M., Mihalopoulos, N., Kouvarakis, G., Jennings, S. G., O'Dowd, C., Birmili, W., Wiedensohler, A., Weller, R., Gras, J., Laj, P., Sellegri, K., Bonn, B., Krejci, R., Laaksonen, A., Hamed, A., Minikin, A., Harrison, R. M., Talbot, R., and Sun, J.: Explaining global surface aerosol number concentrations in terms of primary

emissions and particle formation, Atmos. Chem. Phys., 10, 4775–4793, doi:10.5194/acp-10-4775-2010, 2010.

Sun, T. S.: Construction, Online-Untersuchung und Modellierung von Parametern zur Beschreibung atmosphärischer Nukleation durch Simulationskammerstudien (COMPASS), Master thesis, Goethe University, Frankfurt/Main, 2013.

COMPASS

B. Bonn et al.

Table 1. Calculated residence time x_τ and standard deviation σ by using the measured CO_2 mixing ratio for flow rates of 10, 15 and 20 L min^{-1} between measurement and reference chamber. The additional flow rate of the CO_2 was (30 ± 1) mL min^{-1}.

flow rate (L min^{-1})	chamber	x_τ (min)	$\sigma(x_\tau)$ (min)
10	COMPASS 1	35.9	0.2
	COMPASS 2	38.4*	0.4*
15	COMPASS 1	26.6	0.4
	COMPASS 2	26.5	0.3
20	COMPASS 1	23.1	0.4
	COMPASS 2	22.3	0.4

* The value was excluded for intercomparison due to external heath impact but is shown for completeness.

Table 2. Calculated deposition rate of gas with the measured CO_2 mixing ratio at the inlet and outlet region of the chamber.

Chamber	vmr (inlet) (ppmv)	vmr (outlet) (ppmv)	$k_{dep,gas}$ (s^{-1})	$\Delta k_{dep,gas}$ (s^{-1})
COMPASS 1	828.3 ± 6.3	815.2 ± 3.3	1.0×10^{-5}	5.4×10^{-6}
COMPASS 2	752.4 ± 8.7	734.1 ± 3.2	1.6×10^{-5}	7.8×10^{-6}

Full Screen / Esc

Printer-friendly Version

Interactive Discussion

Table 3. Impact of solar radiation and ozone on VOC mixing ratios observed. Bold marked values indicate significant changes.

Molar mass	Compound	COMPASS 2/COMPASS 1 at elevated ozone			COMPASS 2/COMPASS 1 at elevated. O_3 and reduced radiation		
		Night-time (%)	day-time (%)	all (%)	Night-time	day-time	all
30	Formaldehyde	**+31.5 ± 19.7**	**+20.0 ± 11.1**	**25.5 ± 16.0**	**+48.3 ± 6.4**	**+35.4 ± 12.4**	**+39.8 ± 12.3**
32	Methanol	**+4.5 ± 4.1**	+2.7 ± 3.2	+3.3 ± 3.4	**−7.4 ± 2.6**	**−10.1 ± 4.0**	**−9.1 ± 3.8**
44	Acetaldehyde	**+11.7 ± 5.0**	**+8.4 ± 5.9**	**+9.9 ± 5.4**	**+5.6 ± 2.5**	+5.8 ± 5.8	**+5.7 ± 4.9**
46	Formic acid	−0.4 ± 2.4	+0.6 ± 11.1	−0.2+ 2.5	+1.8 ± 2.0	+1.6 ± 4.0	+1.7 ± 3.5
58	Acetone	**+9.6 ± 5.1**	+5.0 ± 5.2	**+6.9 ± 5.3**	**+4.7 ± 2.0**	**+5.2 ± 4.5**	**+5.0 ± 3.8**
60	Acetic acid	**−9.1 ± 6.8**	−7.6 ± 9.5	**−8.8 ± 5.7**	**+10.4 ± 5.4**	+4.9 ± 8.4	+6.8 ± 8.0
66	Cyclo-pentadiene, malononitrile	−9.4 ± 33.3	−5.4 ± 30.8	−6.7 ± 31.6	+11.4 ± 53.9	+21.5 ± 49.4	+18.0 ± 51.1
68	Isoprene	+1.3 ± 7.8	+2.1 ± 8.1	+1.6 ± 7.6	+0.8 ± 6.0	+1.3 ± 7.4	+1.1 ± 6.9
72	1-propene, butanal, 2-butanone	**+13.7 ± 9.4**	**+7.6 ± 7.3**	**+10.5 ± 8.3**	+2.6 ± 3.6	+2.9 ± 5.2	+2.8 ± 4.7
78	Benzene	+23.4 ± 39.8	+20.0 ± 37.5	+21.8 ± 31.3	+25.6 ± 34.0	+25.9 ± 38.4	+25.8 ± 36.8
81[*]	MT fragment	−5.0 ± 7.3	−1.7 ± 8.5	−3.4 ± 7.6	**−8.4 ± 7.5**	−8.0 ± 9.6	−8.2 ± 8.9
92	Toluene	−0.5+30.6	+1.9 ± 28.9	+1.3 ± 29.9	−5.8 ± 27.6	+4.9 ± 25.2	±0 ± 26.3
136	Monoterpenes (MT)	−5.2 ± 15.5	−1.9 ± 16.0	−3.4 ± 15.3	−7.7 ± 15.3	−11.7 ± 16.9	−10.3 ± 16.4
138	Nopinone, sabinaketone	+5.7 ± 44.3	+2.5 ± 40.9	+4.3 ± 43.5	+11.9 ± 46.3	+7.7 ± 41.5	+9.2 ± 43.2
152	Methylsalicylate	+24.6 ± 80.3	+15.4 ± 84.7	+17.4 ± 82.0	+22.8 ± 88.2	+31.9 ± 94.6	+28.8 ± 92.2
154	Linalool	+8.6 ± 50.3	+1.9 ± 46.8	+3.75 ± 46.5	+1.6 ± 36.6	−0.3 ± 32.1	+0.4 ± 33.6
204	Sesquiterpenes	−7.0 ± 36.1	−7.0 ± 36.1	−7.2 ± 37.3	+5.5 ± 31.6	+7.5 ± 36.9	+6.8 ± 35.1

[*] Primary fragment ion of monoterpenes (MT).

Table 4. Impact of monoterpene (β-pinene) addition on VOC mixing ratios observed. Bold marked values indicate significant changes. Sesquiterpene (β-caryophyllene) addition did not show any significant changes due to high reactivity of SQTs and smaller addition.

Molar mass (g mole^{-1})	Compound	COMPASS 2/COMPASS 1 at elevated MT		
		Night-time (%)	day-time (%)	all (%)
30	Formaldehyde	**+7.0 ± 5.4**	+1.9 ± 7.2	+4.6 ± 6.9
32	Methanol	**−5.8 ± 2.3**	**+6.4 ± 2.6**	**−6.2 ± 2.5**
44	Acetaldehyde	−0.8 ± 2.0	+2.9 ± 6.3	+0.7 ± 5.5
46	Formic acid	−0.4 ± 2.4	+0.5 ± 3.3	−0.1 + 2.8
58	Acetone	−0.5 ± 1.6	+1.5 ± 4.9	+0.8 ± 4.1
60	Acetic acid	−0.2 ± 0.4	0.0 ± 5.4	+0.1 ± 4.9
66	Cyclo-pentadiene, malononitrile	**+217.7 ± 96.6**	**+123.5 ± 30.0**	**+168.9 ± 125.5**
68	Isoprene	**+12.1 ± 7.8**	+5.4 ± 9.5	+9.0 ± 9.2
72	1-propene, butanal, 2-butanone	−0.9 ± 3.6	−0.6 ± 5.8	+0.7 ± 5.0
78	Benzene	+23.7 ± 26.5	+9.3 ± 20.5	+14.3 ± 21.3
81[*]	MT fragment	**+452.8 ± 138.8**	**+204.6 ± 181.2**	**+252.8 ± 210.6**
92	Toluene	**37.1 + 15.5**	+20.0 ± 24.1	**+30.6 ± 22.1**
115	Proline	−4.0 ± 20.2	+0.3 ± 21.2	−0.3 ± 21.4
136	Monoterpenes (MT)	**+461.3 ± 143.5**	**+222.3 ± 190.2**	**+300.1 ± 212.1**
138	Nopinone, sabinaketone	+10.0 ± 12.9	+1.5 ± 15.2	+5.8 ± 15.0
148	MBO, SQT fragment	−0.8 ± 6.5	−0.1 ± 5.9	−0.2 ± 6.1
152	Methylsalicylate	+11.5 ± 67.1	−0.1 ± 40.8	+0.1 ± 42.1
154	Linalool	+2.3 ± 23.7	+0.7 ± 21.3	+2.1 ± 22.3
168	Pinonaldehyde, caronaldehyde, limonaketone	+0.6 ± 44.9	+0.3 ± 40.3	+0.3 ± 39.9
204	Sesquiterpenes	+2.2 ± 18.9	−0.8 ± 17.5	−1.4 ± 18.1

[*] Primary fragment ion of monoterpenes.

Discussion Paper | Discussion Paper | Discussion Paper | Discussion Paper |

AMTD

6, 5959–6004, 2013

COMPASS

B. Bonn et al.

Title Page

Abstract | Introduction

Conclusions | References

Tables | Figures

◀◀ | ▶▶

◀ | ▶

Back | Close

Full Screen / Esc

Printer-friendly Version

Interactive Discussion
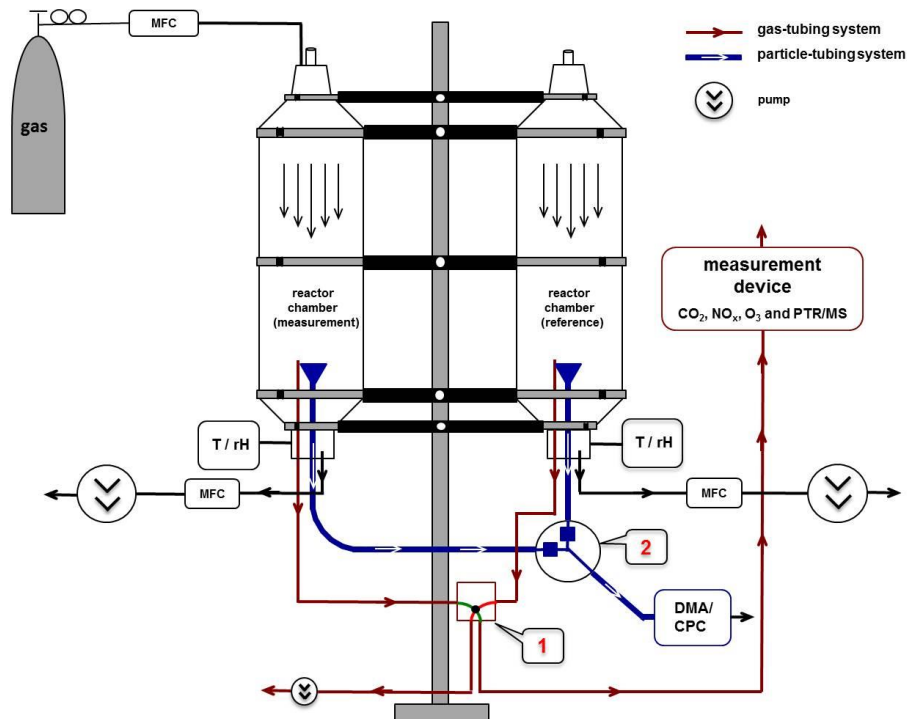
Fig. 1. Flow chart of the COMPASS – system. Valve system 1 (magnetic valve) and 2 (GROTEC-valve) are used for the periodic change of gas and particle sampling between modification and reference chamber.
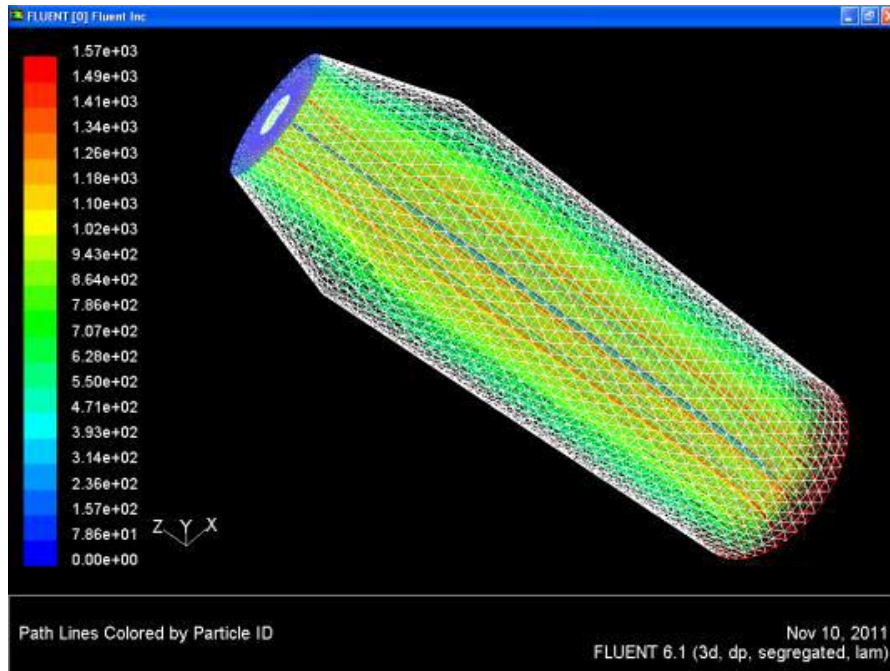
Fig. 2. Flow simulation for the COMPASS – system using the FLUENT 6.1 software.

The figure shows a plot with the following legend and data table:

- × COMPASS_1
- △ COMPASS_2
- – – Exp Fit COMPASS_1_15L/min
- —— Exp Fit COMPASS_2_15L/min

flowrate = 15 L/min

x-axis: time (min), y-axis: normalized CO_2 mixing ratio

Model		Exp_1		
Equation		y = A1*exp(-x/t1) + y0		
--	R^2	parameter	value	standarderror
COMPASS_1	0,99	y0	0,99761	0,00195
		A1	-1,96142	0,01726
		t1	19,33396	0,17797
COMPASS_2	0,99	y0	1,03853	0,00336
		A1	-1,70339	0,012
		t1	23,13846	0,2712

Fig. 3. Measured temporal pattern of the normalized CO_2 mixing ratio at the outlet at a flow rate of $15 \, \mathrm{L \, min^{-1}}$ at a sudden CO_2 increase at the inlet. Exponential fitting of the data points for calculation of the residence time.
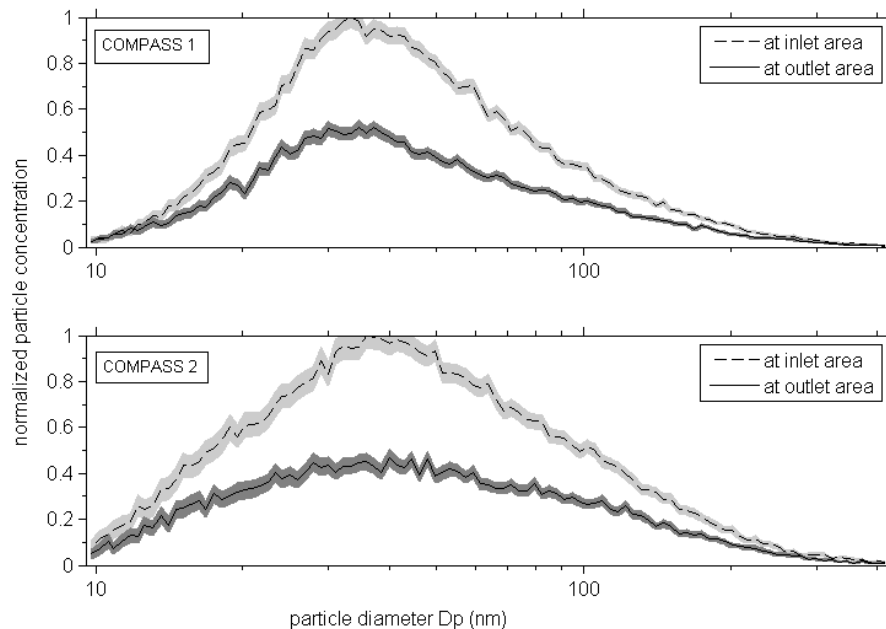
Fig. 4. Observed normalized particle number and volume concentrations at the inlet and outlet of the reference (COMPASS 1) and modification chamber (COMPASS 2). Normalization was based on the maximum of COMPASS 1.
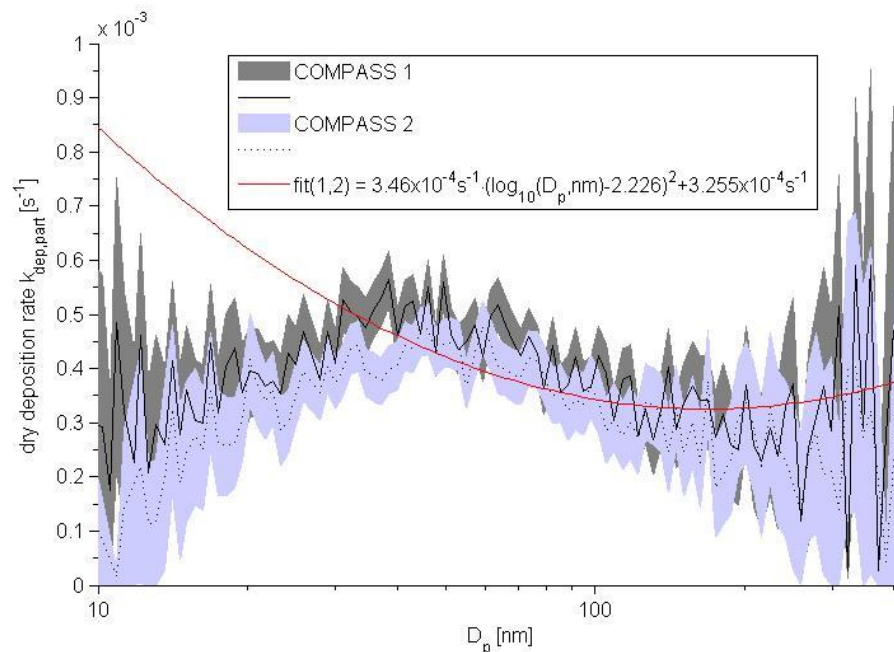
Fig. 5. Dry particle deposition rate kdep,part inside measurement and reference chamber as a function of the particle size. The uncertainty ranges is displayed by the shaded areas. The fit for the average values of both chambers between 50 and 422 nm is shown in red.
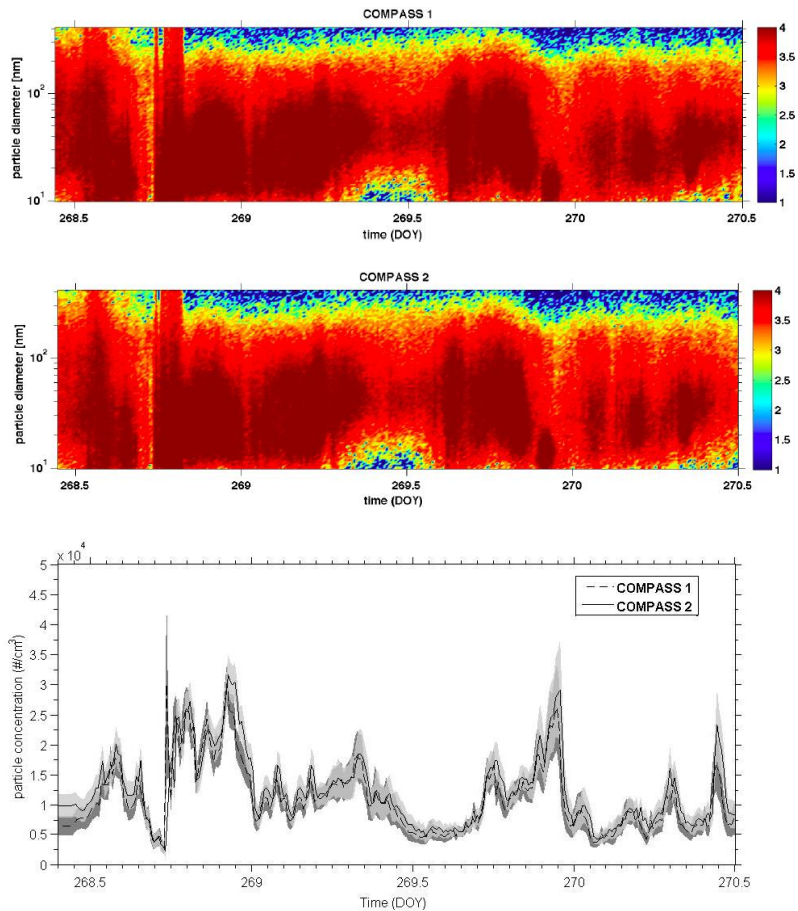
Fig. 6. Top and center plot: particle size distribution dN/dlog(D_p) at non-modified conditions for both chambers to indicate similarity (DOY 268–270, 2012). The colour bar is logarithmic scaled. Bottom: same for total particle number concentration.
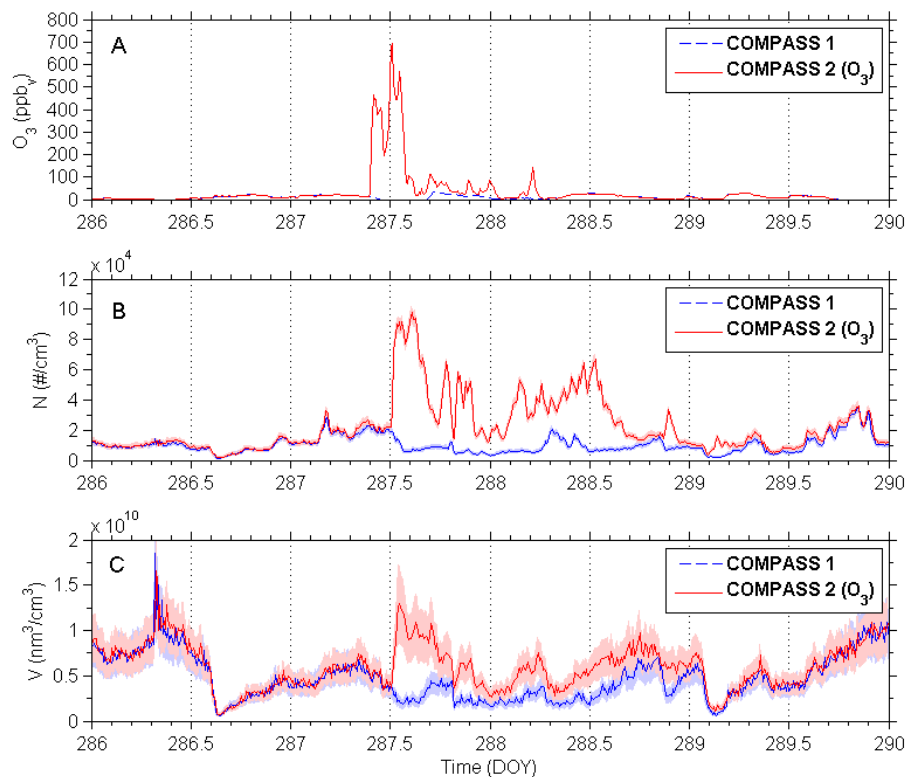
Fig. 7. Urban air (Frankfurt/Main): Ozone mixing ratio **(A)**, particle concentration **(B)** and particle volume concentration **(C)** during the ozone enhancement experiment (DOY 286–290). The ozone mixing ratio was increased in chamber 2 by pen ray ($\lambda = 253.7$ nm).
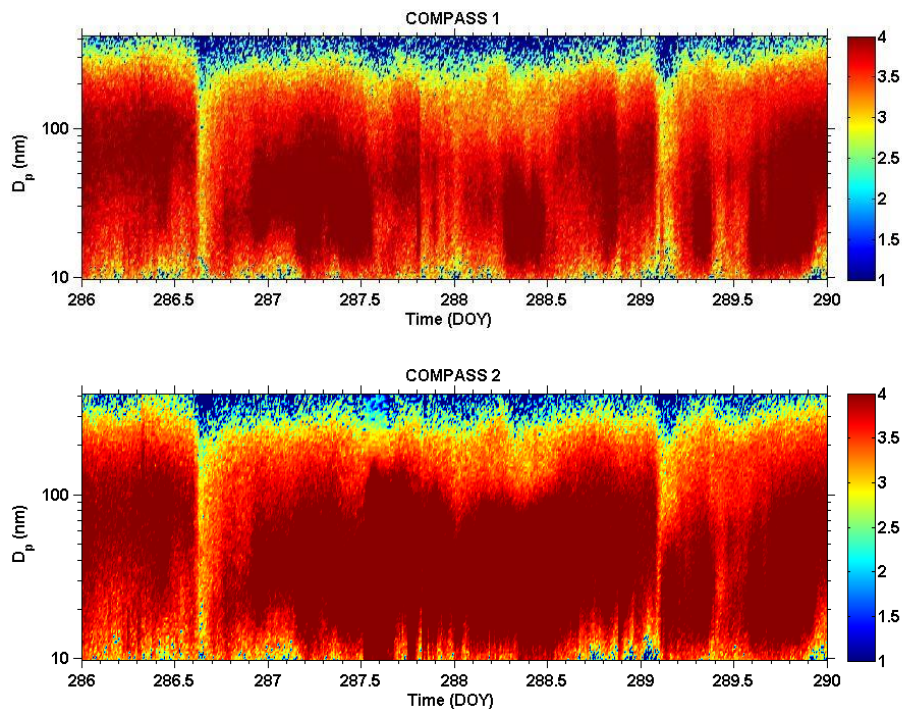
Fig. 8. Particle size distribution plots during the urban ozone enhancement experiment between the modified (COMPASS 2, lower plot) and reference chamber (COMPASS 1, upper plot). The colour bar displays the logarithmic scaled dN/dlog(D_p) values.
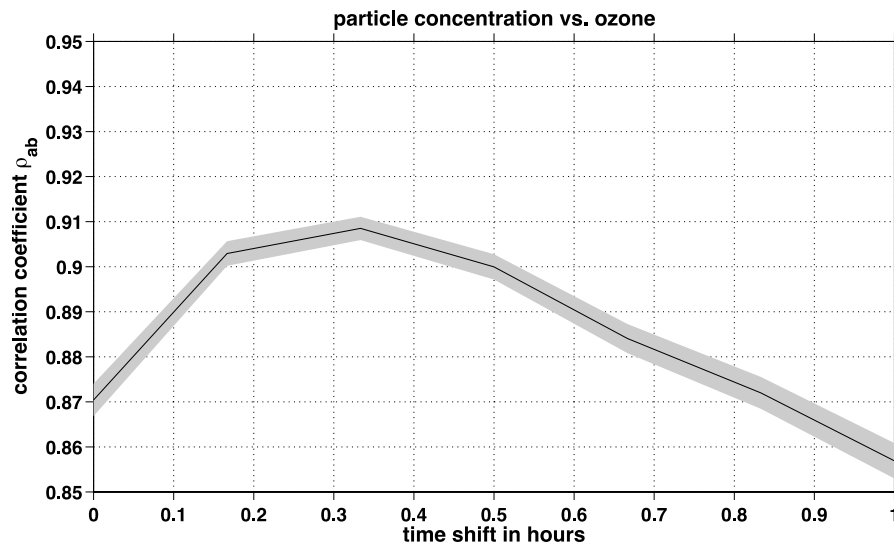
Fig. 9. Cross-correlation of measured particle number concentration and ozone volume mixing ratio difference between COMPASS 2 (modified) and COMPASS 1 (reference) during the ozone enrichment experiment (DOY 286–290, 2012).
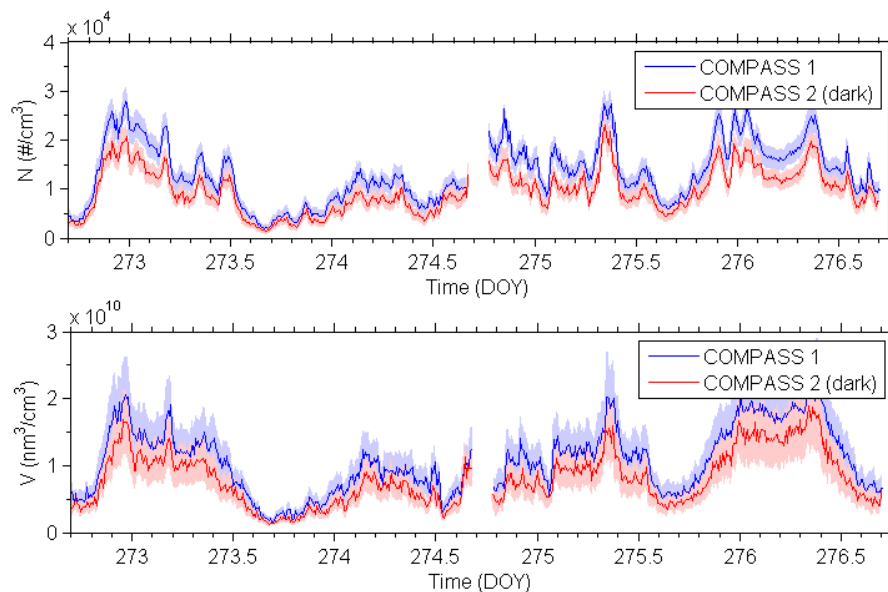
Fig. 10. Particle number and volume concentration measurements during the period during which COMPASS 2 was shaded from sunlight at urban conditions.
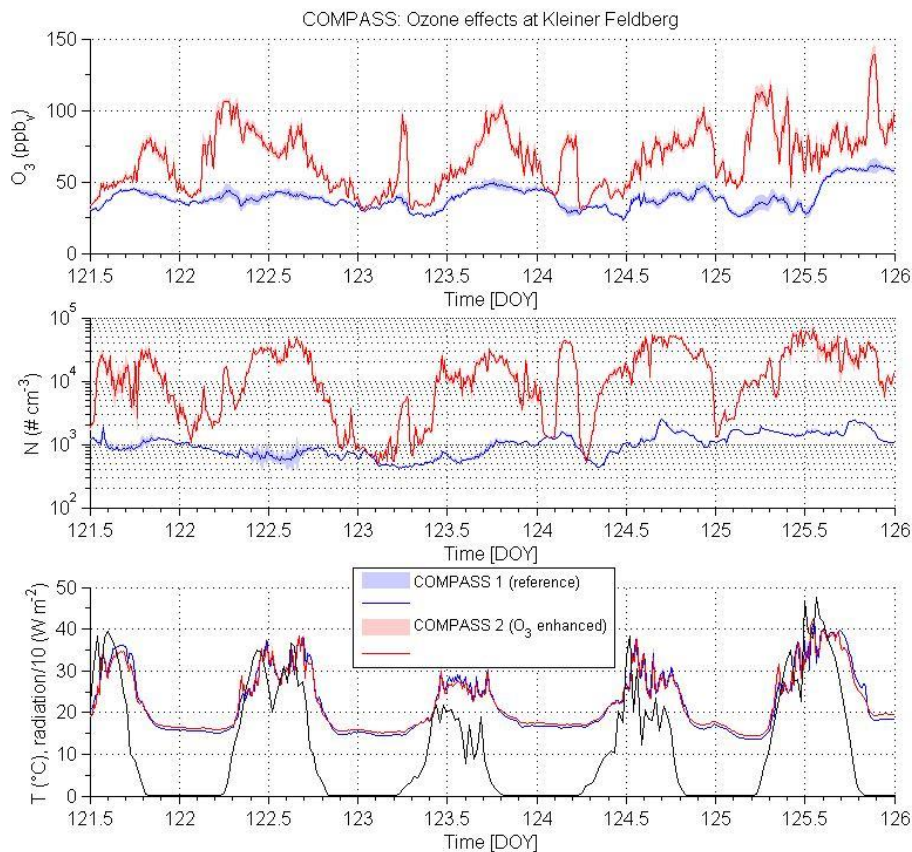
Fig. 11. Remote conditions at Taunus Observatory, Phase I: (top) Ozone mixing ratio in COM-PASS 1 (reference) and COMPASS 2 (Ozone enhancement). (center) Particle number concentration during the ozone increase experiment in both chambers and (bottom) temperature and global radiation in both chambers.
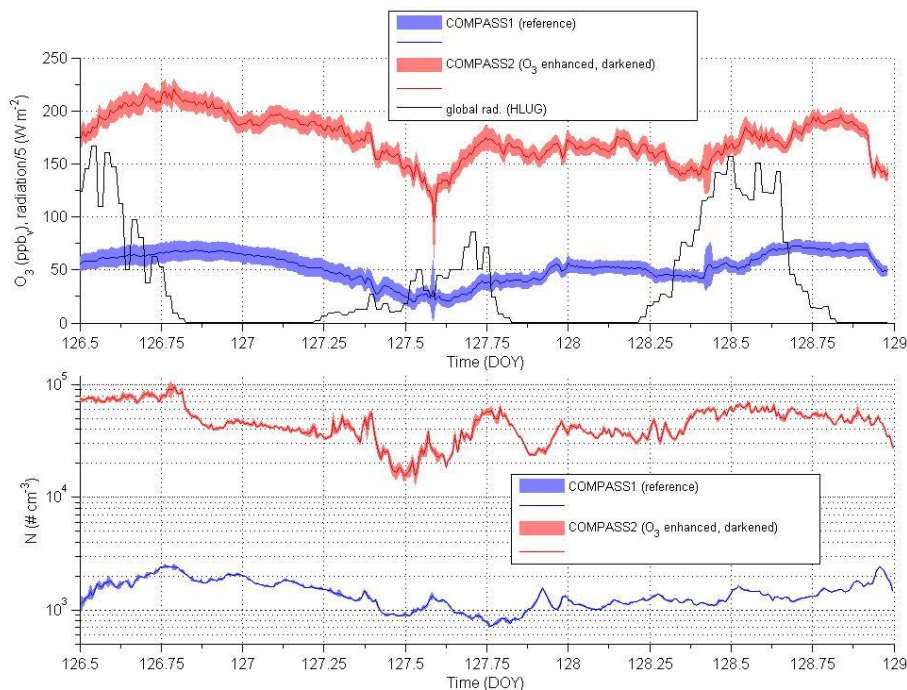
Fig. 12. Ozone enhancement and reduction of solar radiation in COMPASS 2 at Taunus Observatory, Phase 2: (top) Ozone mixing ratios in COMPASS 1 and 2 as well as global radiation at the site of interest. (bottom) Effect on particle concentration measured.
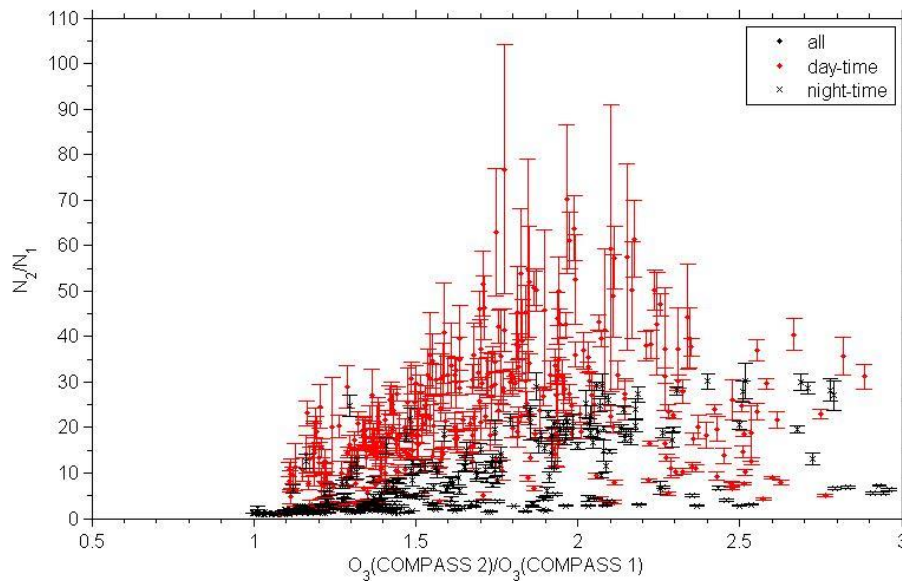
Fig. 13. Scatter plot of relative ozone vs. relative particle number increase at different times in COMPASS.
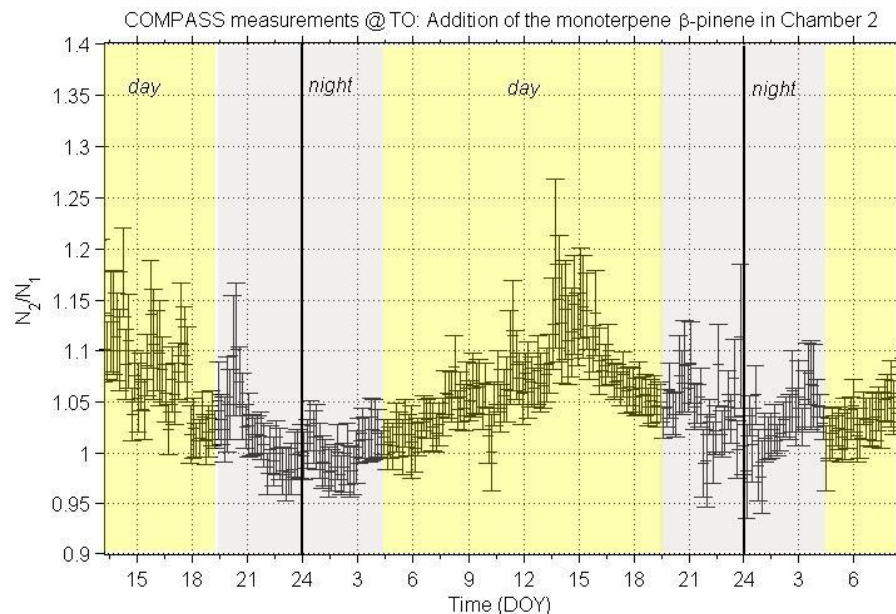
Fig. 14. Phase III: experiment with external monoterpene (upper plot) supply to COMPASS 2. Upper plot: monoterpene mixing ratio at the end of each chamber. Bottom plot: displayed is the ratio of 10 min averaged particle number concentrations of COMPASS 2 to COMPASS 1.
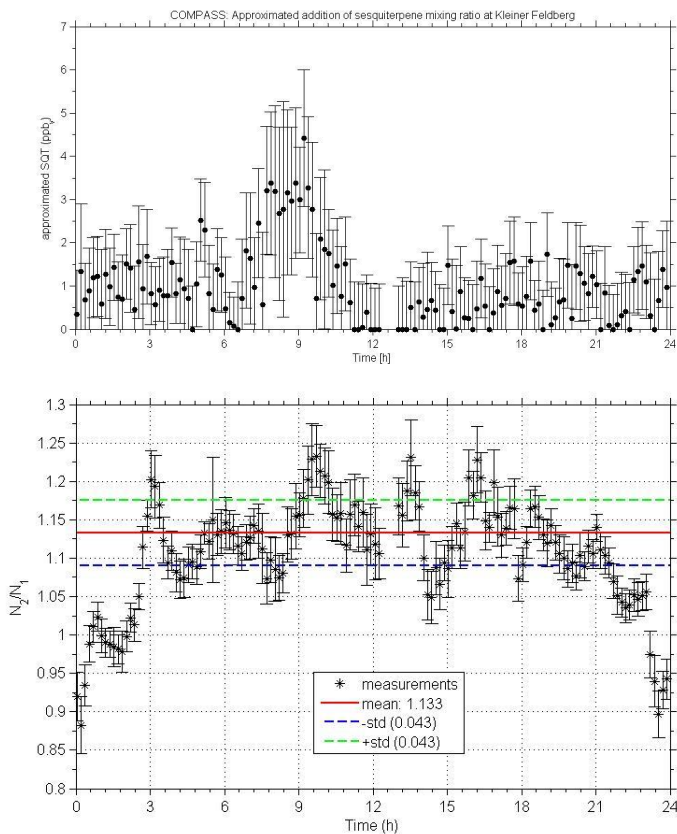
Fig. 15. Phase IV: experiment with external sesquiterpene supply to COMPASS 2. Upper plot: additional sesquiterpene mixing ratio as approximated by the difference in ozone mixing ratio between both COMPASS chambers (reference-modified one). Bottom plot: displayed is the ratio of 10 min averaged particle number concentrations of COMPASS 2 to COMPASS 1. Note the time shift due to the residence time in the chamber by ca. 0.5 h.
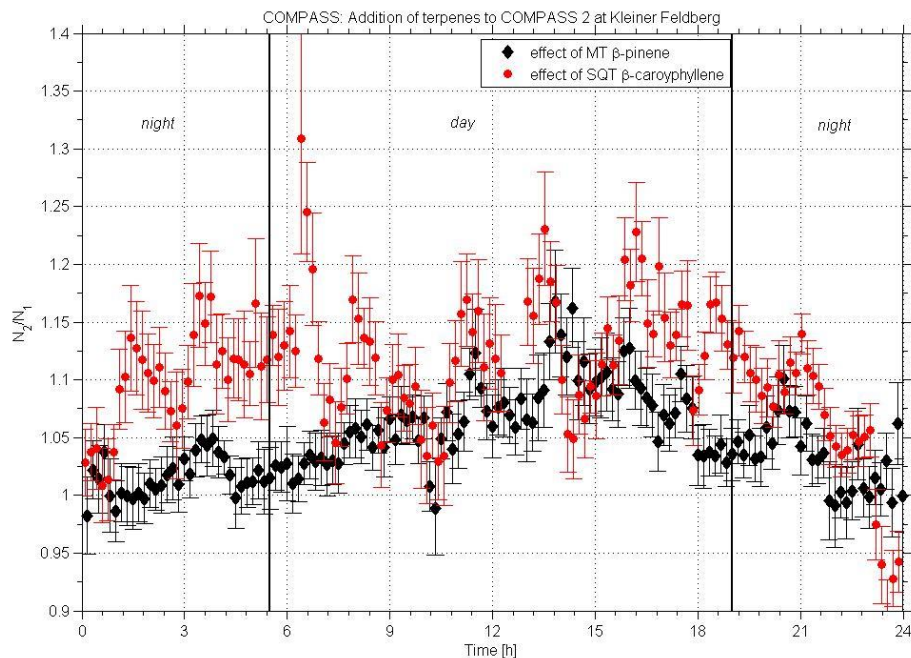
Fig. 16. Daily pattern of particle number concentration ratio of both chambers during both terpene additions, i.e. (a) β-pinene (MT, OH-reactive) and (b) β-caryophyllene (SQT, ozone reactive).